

Institute of Marine and Atmospheric Research Utrecht, University of Utrecht, Utrecht, The Netherlands

The Synoptic Setting of a Thundery low and Associated Prefrontal Squall Line in Western Europe

A. van Delden

With 17 Figures

Received February 3, 1997

Revised October 31, 1997

Summary

A case study of a thundery low and associated prefrontal squall line in western Europe is presented. It is shown that the prefrontal squall line is linked to the vertical circulation associated with an intensifying cold front and a propagating midtropospheric jetstreak, with maximum wind speeds at levels between 700 and 500 hPa. The squall line is triggered in the updraught of the cross-frontal circulation, which can be observed at the earth's surface as a line of mass convergence or confluence stretching for more than 1000 km from southern Iberia to northern France. The intensification of the front and the destabilization of the atmosphere are interpreted by using the slope of isentropes as indicator of frontal intensity. An equation is derived for the rate of change of frontal intensity, which predicts a forward tilt of the cold front with increasing height due to the cross-frontal circulation in the area of warm air advection (the so-called Spanish plume) and, associated with this, a destabilization of the atmosphere at mid-tropospheric levels.

1. Introduction

The most intense thunderstorms in Western Europe, as far as rainfall is concerned, are those which form in the Mediterranean area in autumn, when the sea surface temperature exceeds 25 °C. These so-called mesoscale convective systems, which frequently cause flash floods in the coastal mountainous areas of Spain, France and Italy (e.g., Sényesi et al., 1996), are usually triggered by the large scale lifting of air to the east or north of

a cold core cut-off low or trough entering the Mediterranean (Ramis et al., 1994). They can become very severe due to the strong potential static instability over the Mediterranean Sea and due to orographic lifting. A second distinguishable type of thunderstorm in Europe is the thunderstorm, having supercell characteristics, which is observed principally over the higher ground to the north of the Alps in spring and summer. This type of thunderstorm not seldomly is accompanied by damaging hail (Heimann and Kurz, 1985; Höller and Reinhardt, 1986; Schmid et al., 1997). A third distinct class of severe thunderstorms occurring in western Europe resembles a "prefrontal" squall line. It is observed most frequently over France (particularly the south west of France), Germany and the Benelux, from April to September. It is triggered at a line of convergence or confluence at the earth's surface, which tends to form ahead of a cold front. This paper is concerned with a case-study pertaining to the latter class of thunderstorms.

The first paper to treat extensively the special synoptic setting of thunderstorms in western Europe was written by Carlson and Ludlam (1968). They identified the so-called *Spanish plume* as an important synoptic scale feature promoting the formation of severe thunderstorms in the UK (see also Morris, 1986). This plume of

relatively dry and warm air is formed over the Spanish plateau at levels between 900 and 700 hPa. Under influence of an approaching trough over the Atlantic ocean this air is advected toward the north over the Bay of Biscay and France where large amounts of water vapour can accumulate in the boundary layer, because the Spanish plume acts as a capping inversion preventing deep convection. Above the Spanish plume high levels of potential static instability are created. In the American literature this thermodynamic state of the atmosphere is called “the loaded gun”. A forcing mechanism is needed to “let the gun go off”, i.e. to lift the air in the boundary layer to its level of free convection.

In recent years more investigations, concerned with the broader scale thermodynamic and dynamic setting of thunderstorms in Western Europe have appeared in the literature. S en esi et al. (1996) have described a thunderstorm of the first type mentioned above affecting France; Browning and Hill (1984), Morris (1986), McCallum and Waters (1993), Browning and Roberts (1994), Collier and Lilley (1994), Galvin et al. (1995) and Young (1995) have described thunderstorms affecting the United Kingdom; Heimann and Kurz (1985), H oller and Reinhardt (1986), Kurz (1993), H oller (1994), Prenosil et al. (1995) and Haase-Straub et al. (1997) have described thunderstorms affecting Germany; Huntreisser et al. (1995), Schiesser et al. (1995) and Schmid et al. (1997) have described thunderstorms affecting Switzerland; Ramis et al. (1995) have described thunderstorms affecting Spain; Alberoni et al. (1996) have described thunderstorms affecting Italy, and van Delden (1992, 1994) has described thunderstorms affecting the Netherlands.

The general belief in the Netherlands is that the most severe thunderstorms affecting the Netherlands are embedded in a so-called “thunderly low”, which in the first instance is a heat low formed by strong solar heating of the land surface, principally over the Iberian plateau, and is later intensified by geostrophic forcing when a trough and, frequently, an associated upper level jetstreak approaches the continent from the west. Within the thunderly low thunderstorms usually develop along a line of surface confluence or convergence, giving the system the

appearance of a squall line (see e.g., van Delden, 1994).

The thunderly low usually appears first over the north Iberian plateau and subsequently moves towards France. It is by no means a rare phenomenon: according to the climatology of cyclogenesis published by Petterssen (1956), northern Iberia is the seat of the highest frequency of surface cyclogenesis in summer in the European area.

The origin of the thunderly low and the associated nonfrontal line of surface confluence or convergence, which usually is more than 1000 km long, stretching from southern Spain to northern France, is not clear. In this paper we intend to show that the line of confluence or convergence is the manifestation at the earth’s surface of a vertical circulation forced by thermal wind adjustment of the cold front near the earth’s surface as it moves eastward and approaches an area of intense low level warm air advection over Iberia and France. It will be shown that the vertical circulation itself intensifies the front and destabilizes the atmosphere at upper levels in the region of warm air advection. A jetstreak develops over Iberia with a maximum intensity at about 5000 m above sea-level. The thunderstorms are triggered first in the vicinity of this mid-tropospheric jetstreak.

We will illustrate this process, and other synoptic dynamical processes associated with the formation and intensification of the thunderly low and the subsequent development of severe squall line thunderstorms, with the case of August 8, 1992, employing satellite imagery, synoptic observations and ECMWF analyses. We will especially focus on the upper level and lower level sources of lift and potential static instability.

We will introduce a new definition of frontal intensity and frontal intensification, which turns out to be very useful in the interpretation of the events leading up to the formation of the squall line and the associated thunderly low.

2. Area of Interest and Data

Figure 1 shows a map of the area of interest with the main geographic features. The most noteworthy features within the context of this study are the Iberian Peninsula with its 500–1000 m

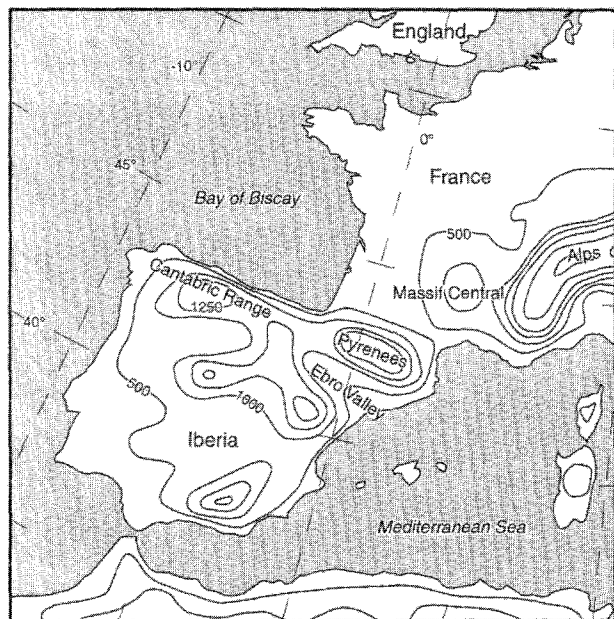


Fig. 1. Map of the area of interest with main topographic features. The orography is smoothed according to the orography in the ECMWF analysis-model system. Isopleths of the height are labeled in metres (500, 1000, 1250, 1500, 2000, 2500)

high relatively dry plateau and the mountain ranges, i.e. the Iberian Range (with peaks slightly higher than 2000 m), the Cantabric Range (with peaks slightly higher than 2500 m) and the Pyrenees (with peaks higher than 3000 m). Further to the north we encounter the Massif Central in central France (with peaks just under 2000 m). Between the Pyrenees and the Massif Central there is a corridor or large valley running between the Mediterranean sea and the Bay of Biscay. Another important valley, also linking the Mediterranean Sea and the Bay of Biscay, is the Ebro valley, which separates the Pyrenees to the north from the Iberian Range to the south.

The data used are Meteosat satellite images, three hourly surface observations and six hourly ECMWF-analyses on a grid with a grid distance of 1° in both horizontal directions on 11 standard pressure levels.

We will first discuss the course of events on August 8, 1992 using satellite images and analyses of synoptic observations made at the earth's surface. Then we will turn to the conditions at upper levels using the ECMWF-analyses.

3. Satellite Images

Figure 2 shows a series of Meteosat satellite images in the infrared channel taken between 0530 and 1730 UTC on August 8, 1992. The first image, corresponding to 0530 UTC, shows a band of high clouds associated with a cold front lying over the western part of Iberia. About five hundred kilometres to the east (along the western edge of France and eastern edge of Iberia) an irregular line of scattered clouds can be observed. Over north-western France and the Bay of Biscay some dissipating thunderstorm clouds can be seen (compare Fig. 2a and 2b). These thunderstorms had formed over northern Iberia on the previous day. At 1330 UTC (Fig. 2c) the band of high clouds associated with the cold front has advanced in easterly direction by about 250 km. Over northern Iberia and the Bay of Biscay the first deep convective clouds have formed in advance of the front. Within a few hours (Fig. 2d) these convective clouds grow to form a line of severe thunderstorms. At the same time the frontal clouds disappear (compare Fig. 2c and 2e).

The explosive growth of convective clouds appears to germinate in the Spanish Basque country and the western Pyrenees. Figure 3 shows a sequence of Meteosat images in the visible channel of this area clearly showing the explosive growth of convective clouds which took place on August 8, 1992. The region shown is centred around the Basque country and spans a distance of about 400 km in west-east direction and about 600 km in south-north direction (see the lower right pannel in figure 3). The first cumulus clouds associated with the squall line form at about 1100 UTC just west of the city of Bilbao near the northern coast of Spain. After about 2 hours new thunderstorm clouds start to form successively to the south, presumably along a line of convergence/confluence at the earth's surface, forming a squall line.

4. Conditions at the Earth's Surface

The reason for the preference for thunderstorm development of this particular area can be understood with the help of an analysis of the observations near the earth's surface. Figure 4 shows maps with the analysis of the sea level

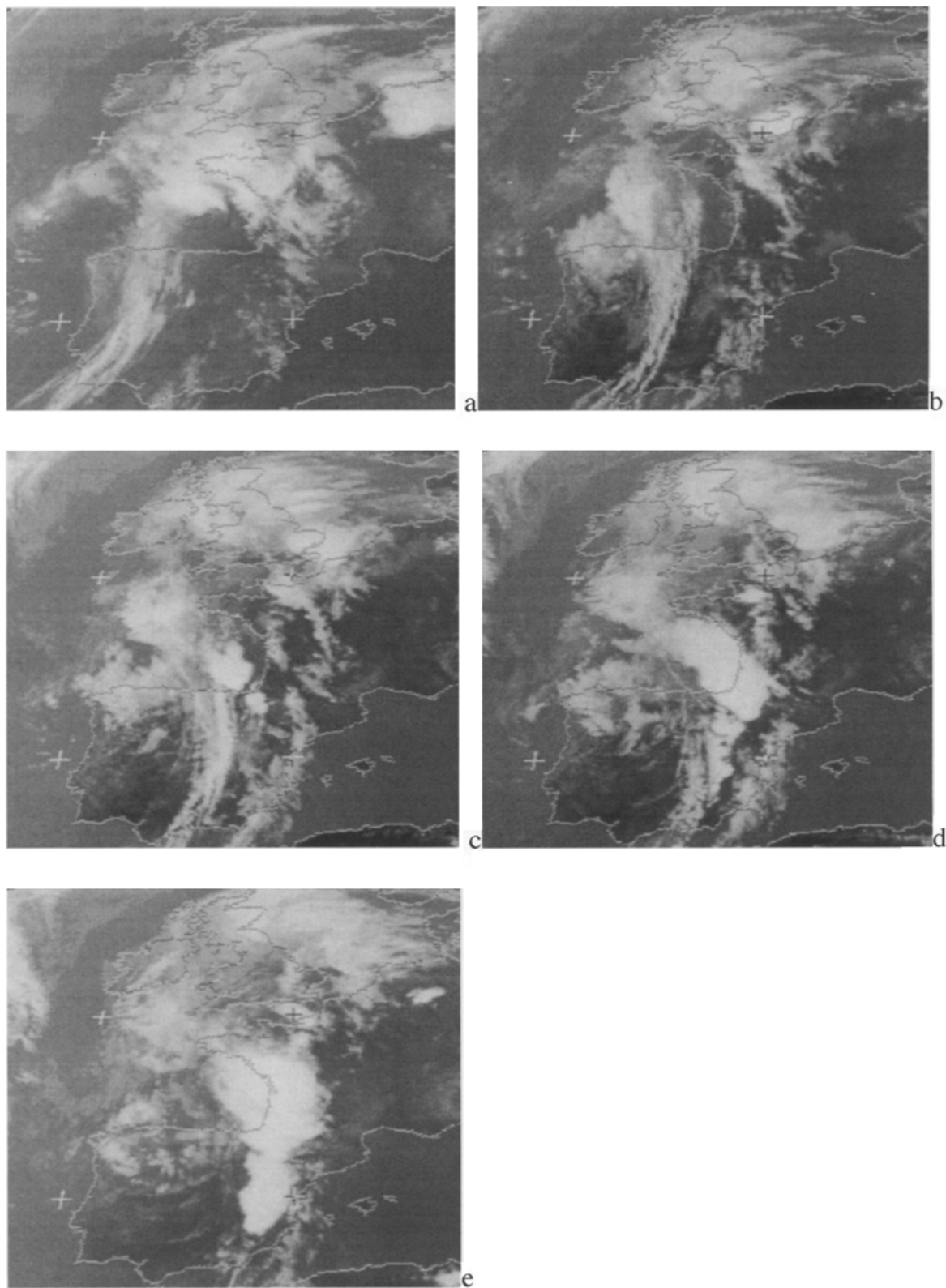


Fig. 2. Meteosat satellite images (infrared) of south-western Europe, corresponding to August 8 1992: (a) 0530 UTC; (b) 1130 UTC; (c) 1330 UTC; (d) 1530 UTC; (e) 1730 UTC

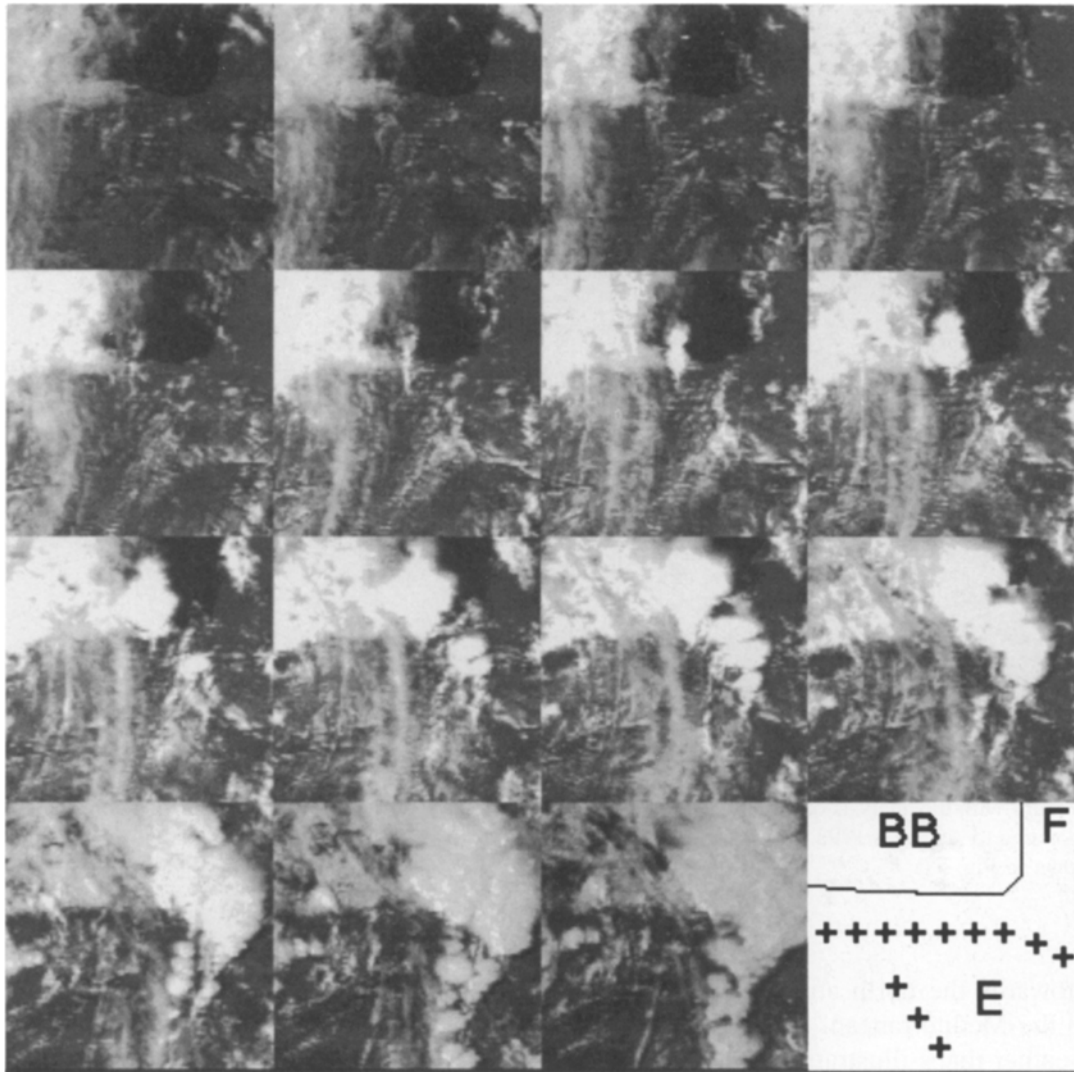


Fig. 3. Overview of Meteosat images made in the visible channel of the area around Basque country (longitude: -5.25° – 0° ; latitude: 39° – 44.5° N). Images shown were taken every half hour starting on 8 August 1992, 9:00 UTC (top/left). Time increases from left to right and from top to bottom. The last image (lower right) corresponds to August 8 1992, 16:00. In the lower right panel the principle geographical features are shown. The letters 'BB', 'E' and 'F' stand for Bay of Biscay, Ebro valley and France, respectively. The full line represents the coast. The plus signs indicate the mountain ranges, i.e. the Cantabrian range along the north coast of Spain, the Pyrenees along the border of Spain and France and the Iberian range (see also Fig. 1)

pressure at three-hour intervals (see appendix A for further technical details of the analysis method). At 0000 UTC, a sea level pressure minimum is located over northern Iberia. Frequently this minimum is referred to by forecasters as a heat low, or *thundery low* if it contains thunderstorms. The thundery low moves in northerly direction during the following hours, reaching the south western corner of France at 0300 UTC. A relatively intense pres-

sure gradient develops on the eastern flank of the low, over north eastern Iberia and southern France.

The thundery low remains centred in the south western corner of France until 1500 UTC, becoming more elongated as time progresses. At 1800 UTC we observe that the isobars roughly follow the coastline of France and Iberia. Between 1800 UTC and 2100 UTC the thundery low splits in two separate parts, with one part

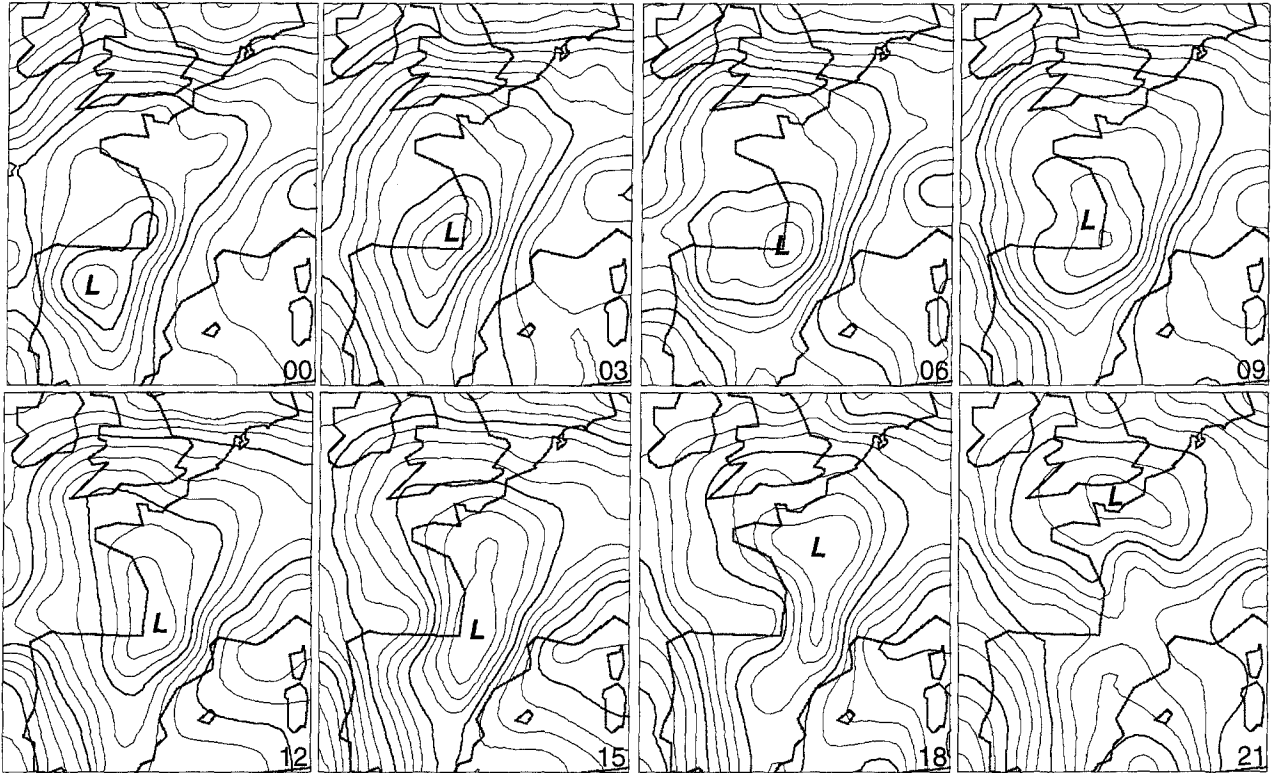


Fig. 4. Three hourly maps with the analysis of the sea level pressure (according to the objective analysis scheme described in appendix A) corresponding to August 8 1992. The time in UTC is shown below in each panel. Isobars are drawn every 1 hPa. More details are shown in Fig. 5

moving further towards the north and the other part moving into the Mediterranean.

The surface weather maps illustrating in more detail the conditions over Iberia and southern France during the formation of the squall line are shown in Fig. 5. A line of mass-convergence or -confluence can clearly be seen running through the axis of the low, stretching from central Iberia into western France. To the west of this line of confluence over Iberia we find warm but relatively dry air, with dew point temperatures ranging from 10 to 15 °C. To the east we find hot, relatively humid air, with dew point temperatures ranging from 17 to 25 °C.

Humid air from the Mediterranean is forced through the great valleys on either side of the Pyrenees (the Ebro Valley to the south and the corridor between the Pyrenees and the French Massif Central to the north) by the strong pressure gradient (see Fig. 4). The highest wind speeds at the earth's surface (approximately 10 to 15 m/s) are observed in the upstream parts of these two valleys.

Another clearly distinguishable air mass in Fig. 5 is the air mass flowing from west to east along the north coast of Iberia and over the Bay of Biscay. This air has a temperature of about 20 °C, which is slightly lower than the *dewpoint* temperature (about 20–25 °C) of the air mass over south western France and the upper Ebro valley at 1200 UTC. Obviously the lifting condensation level of clouds formed in the area where these two air masses meet will be very low. This implies that very little forced upward motion will be needed to generate free moist convection in this area.

Furthermore, an analysis of the average horizontal moisture flux convergence at the earth's surface between 0900 and 1200 UTC (see Fig. 6), calculated from the surface data corresponding to 0900 and 1200 UTC (see appendix B), shows that the greatest moisture flux is found in an oblong shaped area stretching from southern Iberia over the Bay of Biscay, along the western coast of France, over north-western France and then towards East

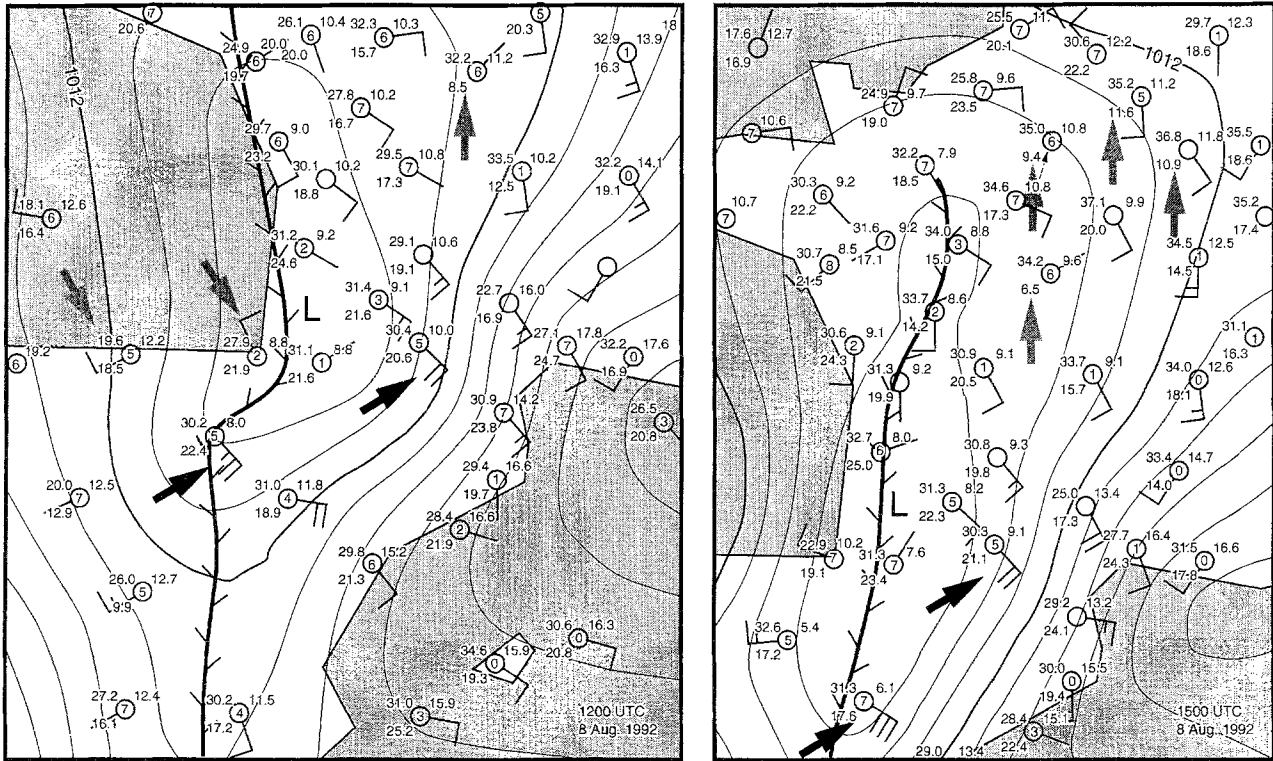


Fig. 5. Surface weather maps corresponding to 1200 (left) and 1500 UTC (right), August 8 1992. The position of a surface station is indicated by a circle. The number inside the circle indicates the cloudiness (in octas). Also indicated are the temperature ($^{\circ}\text{C}$) (upper left), the dew point ($^{\circ}\text{C}$) (lower left) and the pressure (hPa-1000) (upper right). The “hooked” thick solid line indicates the position of the convergence/confluence line. The upward pointing gray arrows highlight the relatively low dewpoints in the north eastern quarter of the thundery low. The slanting upward pointing black arrows highlight high wind speeds. The slanting downward pointing gray arrows highlight the cool humid air flowing towards the east along the steep north coast of Iberia and the hot, very humid air over south western France. Also shown are sea level isobars drawn every 1 hPa (thick line corresponds to 1012 hPa), according to the objective analysis scheme described in appendix A

Anglia. Within this area marked moisture flux convergence is found in the upper Ebro Valley. Many authors have identified horizontal moisture flux convergence at the earth’s surface as an important condition for the triggering deep convection (see e.g., Joe et al., 1995). As can be seen in Fig. 2, the upper Ebro Valley is precisely the area where the most vigorous convection takes place first at about 1130 UTC.

An interesting detail in Fig. 5 is the relatively very dry and hot air observed in the north-eastern quarter of the thundery low. Three stations within this area report dewpoints in order of 10°C , while all other stations in the neighbourhood report dewpoint temperatures that are 5° to 15°C higher. We will give an explanation of this observation later.

5. Jetstreams and Jetstreaks

The large scale flow conditions at middle and upper tropospheric levels about 12 hours prior to the formation of the thunderstorm or squall line are illustrated schematically in Fig. 7, which shows the height of the 300 hPa and the 700 hPa pressure surfaces, according to the ECMWF analyses on 8 August 1992 at 0000 UTC. The thundery low is apparently embedded in a jetstream with a trough over the Atlantic Ocean and a ridge over western Europe.

The vertical structure of the jet-front system on 8 August 1992 at 0000 UTC is shown in Fig. 8. The cross section is taken along the 41° -latitude circle between the longitudes -20° and 5° . Therefore, the section runs from the Atlantic ocean, over the Iberian peninsula (between the

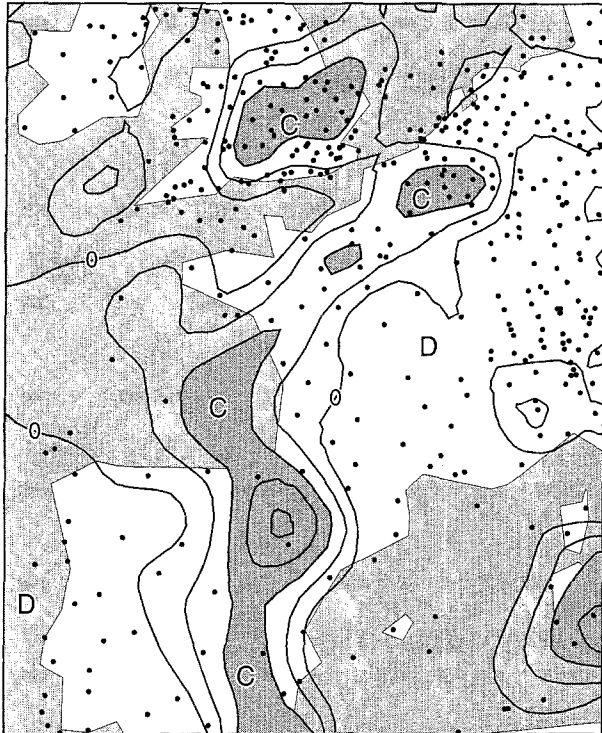


Fig. 6. Average horizontal moisture flux divergence near the earth's surface before the formation of the squall lines on 8 August 1992 between 0900 and 1200 UTC. The average is calculated from the analyses for 0900 and 1200 UTC (the analysis method is described in appendix A and B). Only negative values are contoured. The zero contour is also drawn. The contour interval is $10^{-7} \text{ kg m}^{-3} \text{ s}^{-1}$. Regions where the mean moisture flux convergence is greater than $2 \times 10^{-7} \text{ kg m}^{-3} \text{ s}^{-1}$ are shaded. The letters 'C' and 'D' denote moisture flux convergence and moisture flux divergence, respectively. The black dots indicate the locations of the measuring stations on which the analysis is based. There are over 400 stations within the area shown

longitudes -8.5° and 1°), and finally over the Mediterranean Sea (see Fig. 7). Clearly distinguishable in Fig. 8 is the cold core of the trough at a longitude of about -13° . On either side of this trough we observe two jet cores at a height of about 9 to 10 km. The southerly jet (with winds blowing from the south) on the eastern side of the trough, labeled ULJ₁, is much weaker than the northerly jet (with winds blowing from the north), labeled ULJ₂, on the western side of the trough. In fact ULJ₁ is not the only jet on the eastern side of the trough. There is also a *mid-tropospheric jet core*, labeled MTJ, over Iberia.

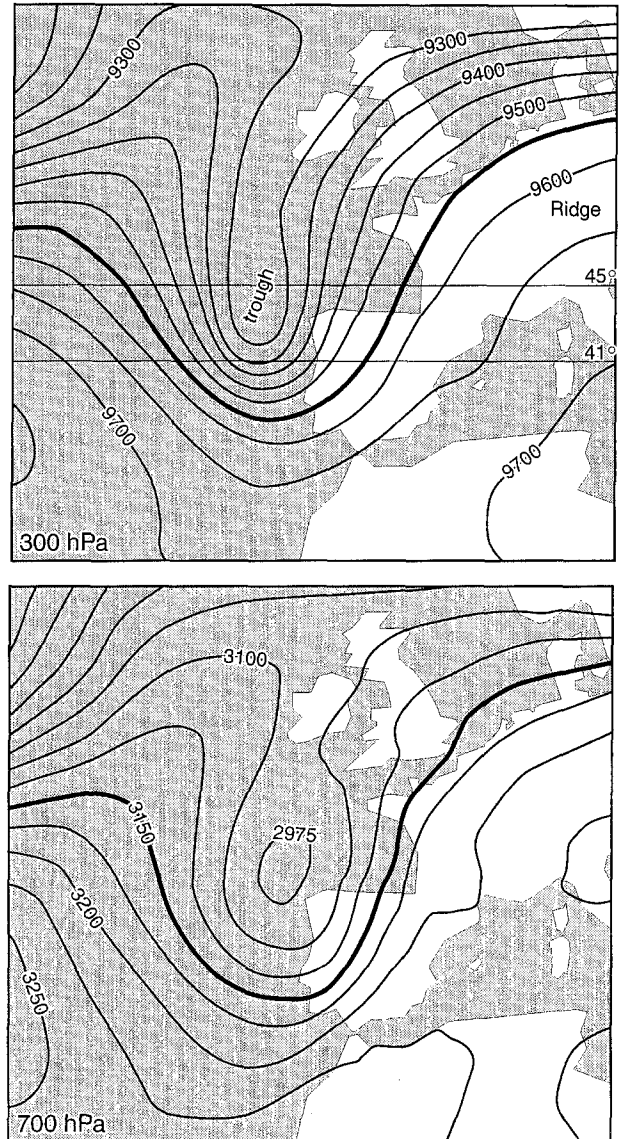


Fig. 7. Analysis (ECMWF) of the 300 hPa height and the 700 hPa height (m) for August 8 1992, 00 UTC. Also shown are the 41° and 45° latitude circles for later reference

Furthermore, although there are no closed isotachs, there is a clear hint of another wind speed maximum, labeled ULJ₃ in Fig. 8, at a height of 12 km above sea level over Iberia.

All these jetstreams are related to thermal fronts via thermal wind balance. ULJ₁ and ULJ₂ are related to the principle upper level (cold) front (UCF) on either side of the trough. ULJ₃ appears to be related to a front at the tropopause in advance (to the east) of the trough, while MTJ is related to an intense low level cold front (LCF) over Iberia. These fronts will be discussed in detail in section 7.

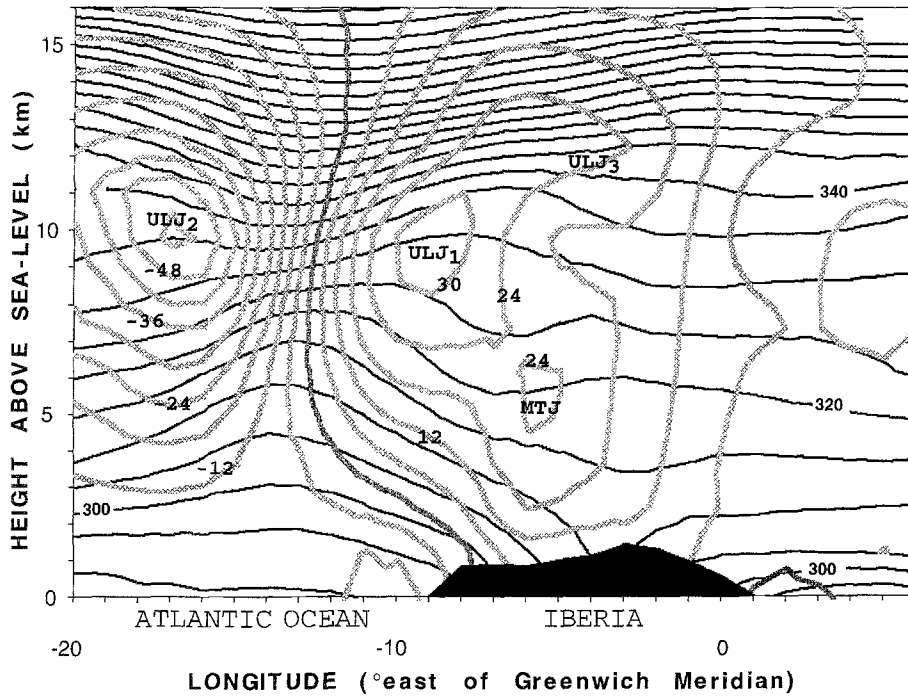


Fig. 8. The potential temperature and the meridional component of the wind velocity as a function of height and longitude for the latitude 41° N, on August 8, 1992, 0000 UTC, according to the ECMWF analysis. Black lines are isentropes drawn every 5 K. Gray lines are isotachs of the meridional wind (v) drawn every 6 $m s^{-1}$. The orography of Iberia, smoothed as in the ECMWF analysis/model, is also shown

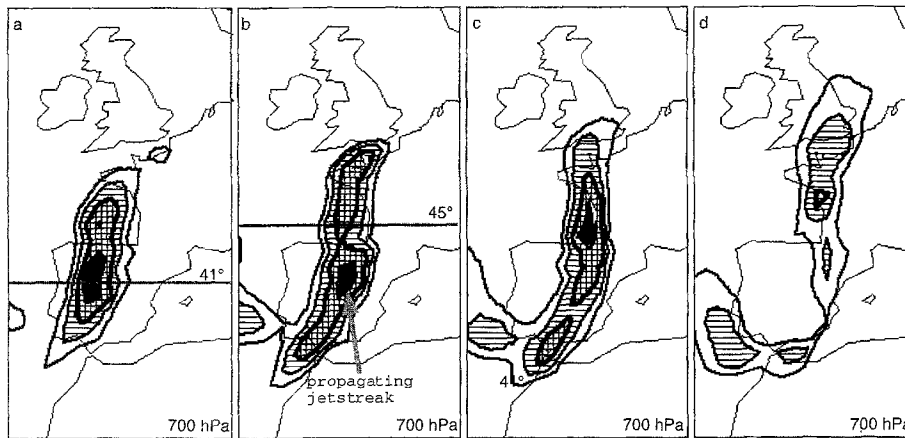


Fig. 9. ECMWF analysis of absolute windspeed at 700 hPa on 8 August 1992, 0000 (a), 0600 (b), 1200 (c), and 1800 UTC (d). Isotachs are drawn every 2.5 m/s, starting at 15 m/s. The thick line corresponds to 20 m/s isotach. Areas where the windspeed is greater than 22.5 m/s are shaded in black

In Fig. 9 it can be verified that the cross section Fig. 8 intersects the most intense part of the jet at 700 hPa (at about 3 km above sea level). In fact, a *jetstreak* is observed at 700 hPa over western Iberia at 0000 UTC on 8 August 1992. This 700 hPa-jetstreak moves in northerly direction through the jetstream during the following hours.

The northward movement of the 700 hPa-jetstreak, observed in Fig. 9, is related to intensification of the lower cold front (LCF) within the atmospheric layer between 925 hPa

and 700 hPa along the western coast of France and the simultaneous relative weakening of the LCF within this layer over Iberia. The *adiabatic* processes contributing to this effect are displayed in Fig. 10. The principle *adiabatic* process contributing to the weakening of the LCF over central and southern Iberia is adiabatic cooling due to upward motion on the warm side (to east) of the front (see Fig. 10b). The principle *adiabatic* processes contributing to the intensification of the LCF at the western coast of France are intense horizontal cold advection over the

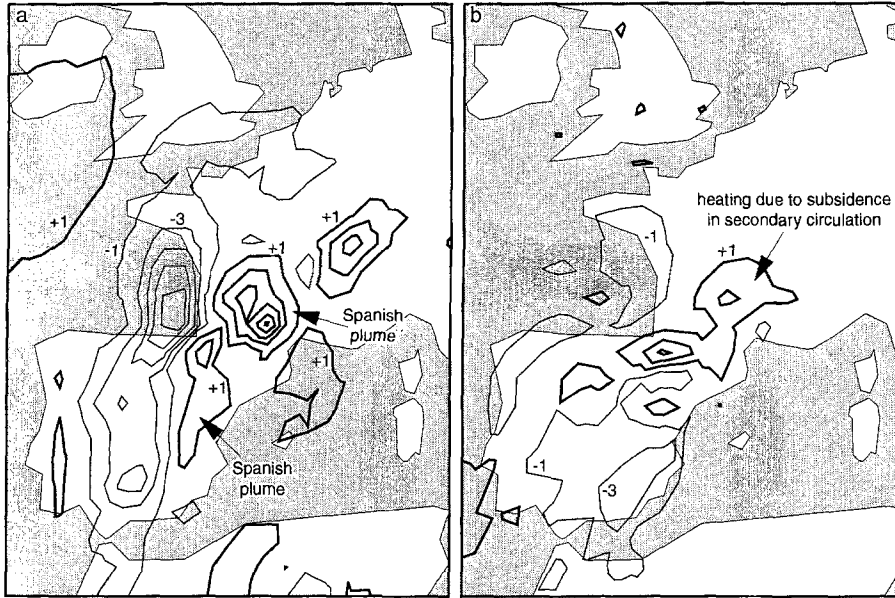


Fig. 10. Mean local tendency of the potential temperature ($\partial\theta/\partial t$) in the layer 925–700 hPa due to (a) horizontal advection of potential temperature ($-u\partial\theta/\partial x - v\partial\theta/\partial y$), and (b) vertical advection of potential temperature ($-\omega\partial\theta/\partial p$), according to the ECMWF-analysis of 8 August 1992, 0600 UTC. The isopleths are labeled in units of 0.0001 K s^{-1} . The contour interval is 0.0002 K s^{-1} . Thick lines correspond to local warming (positive values of $\partial\theta/\partial t$)

coastal area and the Bay of Biscay and simultaneous warm advection further inland (the actual Spanish plume) (see Fig. 10a). This frontogenetic effect is further intensified by adiabatic cooling along the west coast of France due to upward motion and simultaneous adiabatic warming further inland due to downward motion (see Fig. 10b). The eastern part of the warm Spanish plume is therefore subject to subsidence, thus becoming even warmer. Of course, *diabatic* processes also contribute to intensification or weakening of the LCF, but these processes are unfortunately difficult to quantify.

The area of downward motion within the Spanish plume over southern France is part of a secondary (cross-frontal) circulation, which is required to preserve thermal wind balance in the presence of the intensification of the LCF. This will be demonstrated quantitatively in section 6.

Preservation of thermal wind balance in a region of horizontal warm advection requires a veering of the wind vector with increasing height. Therefore, the southerly wind (blowing from the south) must have an easterly component near the earth's surface turning into a westerly component aloft. This implies that, in the x - z plane (approximately perpendicular to the LCF), the circulation must be such that air flows from land to sea near the earth's surface and from sea

to land aloft. This is clearly confirmed by the cross section of the ECMWF-analysis along the 45° latitude circle (over the Bay of Biscay and France) shown in Fig. 11a. The warm Spanish plume can be recognized in this figure by the dent in the isentropes centred around 1°W at the earth's surface. Within the Spanish plume the flow is from east to west below a height of about 2000 m and from west to east above this height. The circulation is thus cyclonic within the x - z plane because the y -component of the vorticity ($\partial u/\partial z - \partial w/\partial x$) is greater than zero.

In the region of horizontal cold advection, on the other hand, the wind must back with increasing height in order to preserve thermal wind balance. This implies the existence of a circulation, within the x - z plane, of the opposite sign at 0600 UTC just west of coast of France. If we carefully observe the wind vectors (in Fig. 11a) in the zone between 5°W and 2°W at heights between 500 and 3000 m, we can indeed detect an anticyclonic circulation.

The cross-frontal circulation, therefore, has two branches: a cyclonic branch on the east side of the lower cold front and an anticyclonic branch on the west side, over the Bay of Biscay. The western branch does not come out very clearly in Fig. 11a, but comes out most clearly in the field of horizontal divergence, shown in Fig. 11b as a function of longitude and height at

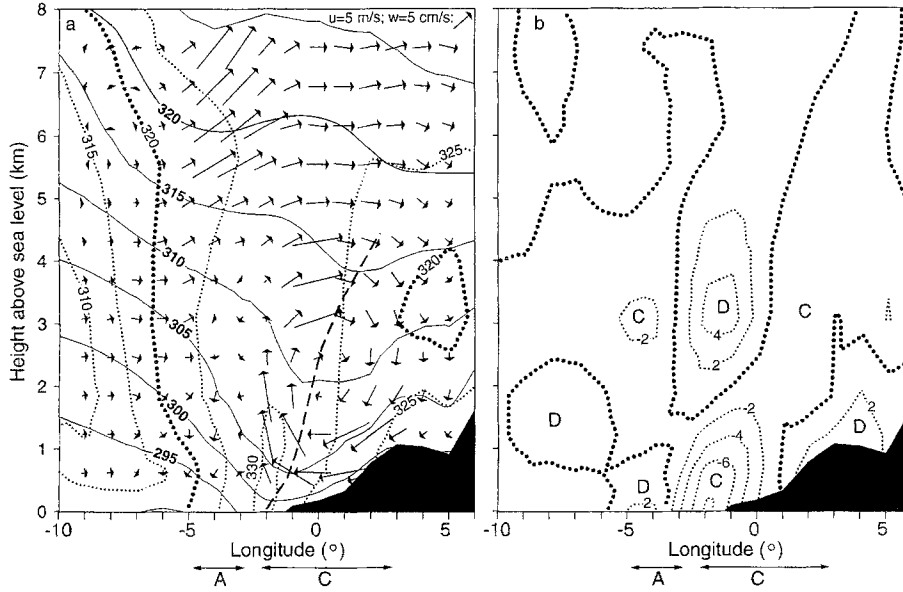


Fig. 11. Vertical cross section along the 45°N latitude circle corresponding to August 8, 1992, 0600 UTC, according to the ECMWF analysis. The orography of France, smoothed as in the ECMWF-model, is also shown. (a) Potential temperature (thin solid lines, labeled in K), equivalent potential temperature (dotted lines, labeled in K) and the component of the wind vector in the plane of the cross section. The dashed line indicates the position of the axis of the Spanish plume. The letters 'A' and 'C' below the horizontal axis indicate the position and extent of the anticyclonic cross-frontal circulation and the cyclonic cross-frontal circulation, respectively. (b) Horizontal divergence (dotted lines, labeled in units of 10^{-5} s^{-1}). The letter 'C' indicates convergence (negative values); the letter 'D' indicates divergence (positive values)

45°N. The line of convergence/confluence at the earth's surface, observed in Fig. 5, is therefore associated with this crossfrontal circulation.

6. Quasi-Geostrophic Analysis of low Level Frontal Intensification

In the previous section we argued qualitatively that the circulation and associated convergence/divergence pattern shown in Fig. 11 is the result of frontal intensification. To first order we can demonstrate this by analysis of the Q-vector, because the Q-vector is proportional to the rate of change, due to the shear and confluence of the geostrophic wind, of the horizontal temperature gradient on an isobaric surface, and because regions where the Q-vector is convergent (divergent) correspond to ascent (descent) (see Holton, 1992, p. 172).

In Fig. 12 the divergence of the Q-vector at 700 hPa according to the ECMWF analysis is shown for 0600 UTC. The 45° latitude circle intersects a region, parallel to the western coast



Fig. 12. ECMWF analysis, corresponding to August 8, 1992, 0600 UTC, of the height of the 700 hPa level (thin solid lines labeled in m) and the divergence of the Q-vector (thick solid lines labeled in units of $10^{-15} \text{ Km}^{-2} \text{ s}^{-1}$)

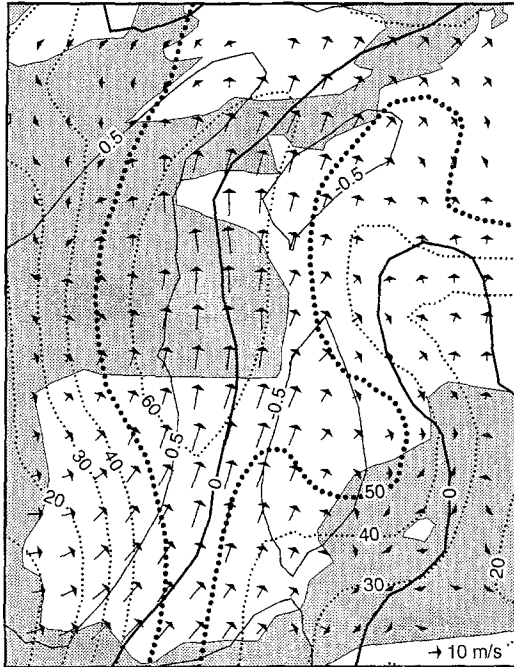


Fig. 13. 700 hPa ECMWF analysis, corresponding to August 8, 1992, 0600 UTC, of the relative vorticity (solid lines labeled in units of 10^{-4} s^{-1}), the specific humidity (dotted lines labeled in units of 0.1 g/kg) and the horizontal wind (arrows; the length is proportional to the speed)

of France, with strong convergence of \vec{Q} (upward motion). On either side of this region there is divergence of \vec{Q} (downward motion). Therefore, quasi-geostrophic Q-vector analysis provides a consistent explanation of the analysis of the circulation pattern, shown in Fig. 11. It is also consistent with the analysis of the moisture field at 700 hPa, shown in Fig. 13, because relatively moist air (usually correlated with upward motion) is observed in the area where \vec{Q} is convergent. In fact, a moist tongue of air can be observed stretching from southern Iberia to the British Isles. A dry tongue, obviously caused by downward motion, is observed over central France. This dry air is later observed also at the earth's surface (see Fig. 5).

In Fig. 13 we can also observe that the vertical component of the relative vorticity at 700 hPa over a large area reaches absolute values exceeding half the planetary vorticity. This implies that the Rossby number in these areas exceeds 0.5, which in turn implies that quasi-geostrophic theory can give no more than an approximate first order explanation of the

existence of vertical circulations due to frontal intensification.

We will see in the following sections that, if we introduce a new definition of frontal intensity, we shall be able to give a consistent and relatively simple explanation of how a vertical circulation, forced due to frontal intensification, can induce further frontal intensification and static destabilization of the atmosphere, promoting convection.

7. Identifying Fronts by the Slope of Isentropes

Since the appearance of the textbook on synoptic meteorology by Petterssen (1940) and the paper on frontogenesis by Miller (1948), the intensity of a front in the atmosphere is usually defined as the absolute value of the horizontal gradient of a scalar such as the potential temperature. This definition is also used in quasigeostrophic theory, from which the Q-vector is derived. However, in Figs. 8 and 11a fronts can be recognized best by observing the slope of isopleths of potential temperature (Fig. 8) or the slope of isopleths of equivalent potential temperature (Fig. 11a). If, indeed, we relate the intensity of a front to the slope of isentropes with a vector, \vec{I}_F , we can write the following:

$$\begin{aligned} \vec{I}_F &= I_{Fx}\hat{i} + I_{Fy}\hat{j} \equiv \left(\frac{\partial z}{\partial x}\right)_\theta \hat{i} + \left(\frac{\partial z}{\partial y}\right)_\theta \hat{j} \\ &= -\left(\frac{\partial \theta}{\partial x} \left[\frac{\partial \theta}{\partial z}\right]^{-1} \hat{i} + \frac{\partial \theta}{\partial y} \left[\frac{\partial \theta}{\partial z}\right]^{-1} \hat{j}\right). \end{aligned} \quad (1)$$

In this equation, θ is the potential temperature, x , y and z are the zonal, meridional and vertical coordinates, respectively, and \hat{i} and \hat{j} are the unit vectors in the x - and y -direction, respectively. We can, if we desire, replace the potential temperature in (1) by the equivalent potential temperature.

Mathematically, this definition differs from the definition due to Miller (1948) only by the factor $-(\partial\theta/\partial z)^{-1}$. The definition according to (1), however, has several advantages compared to the traditional definition due to Miller, which are of importance especially within the context of this study. First, frontal intensity is related to the orientation in space of a material surface, i.e. a

surface of constant potential temperature in dry adiabatic conditions, or a surface of constant equivalent potential temperature in pseudo-adiabatic conditions. This implies that frontal intensification is related to the deformation and rotation of a material surface, which is physically easily to interpret and/or visualize. Second, stable temperature-inversion layers are not considered a front. In fact, according to the above definition, an increase in the vertical (hydrostatic) stability leads to a weakening of the front (lower value of $|\vec{I}_F|$). Third, because the stability of a front (i.e., the linear stability of thermal wind balance) is in fact (see Holton, 1992, p. 237 and p. 280) governed by the slope of the isentropes and not exclusively by the absolute value of the gradient of the potential temperature, $|\vec{I}_F|$ is proportional to the degree of baroclinic stability of a front, and is thus a natural measure of the intensity of a front.

There is one obvious disadvantage: the value of $|\vec{I}_F|$ goes to infinity when $\partial\theta/\partial z = 0$. However, except in the lowest few hundred metres of the atmosphere, $\partial\theta/\partial z$ is nearly always positive everywhere. This problem is more acute, however, when the equivalent potential temperature is used instead of the potential temperature in the definition of frontal intensity (1). This can be seen in Fig. 11a.

In accordance with the alternative definition (1) of frontal intensity, *the position of the front on an isentropic surface* can be defined as coincid-

ing with the ridge in the contour plot of the slope of the isentropic surface. We will apply these ideas to two isentropic surfaces: the 310 K surface, which at 0600 UTC on August 8 1992 descends from a height of about 5000 m over the Atlantic ocean to about 2000 m over western France (see Fig. 14a), and the 320 K surface, which at 0600 UTC on August 8 1992 descends from about 8000 m over the Atlantic ocean to about 6000 m over the Bay of Biscay and western France (see Fig. 14b).

The absolute value of the slope of the 310 K and 320 K isentropic surfaces at 0600 UTC on August 8 1992 as a function of latitude and longitude is shown in Fig. 15. On the 310 K isentropic surface (Fig. 15a) we can distinguish a somewhat fragmented ridge in the slope of this surface, running from the western coast of Iberia to the south west coast of France and then to Normandy. This ridge can be identified with the lower cold front (LCF) connected to the midtropospheric jet (MTJ). The rather variable intensity of the LCF on the 310 K surface can be attributed to the rather variable Iberian topography (see Fig. 1). On the 320 K isentropic surface (Fig. 15b) we can easily recognize two fronts: one running from western Iberia towards the north and the other also stretching in meridional direction along the eastern coast of Iberia into southern France. The front over western Iberia is associated with the upper level jet ULJ₁ (see Fig. 8) and with the cloud band over Iberia seen

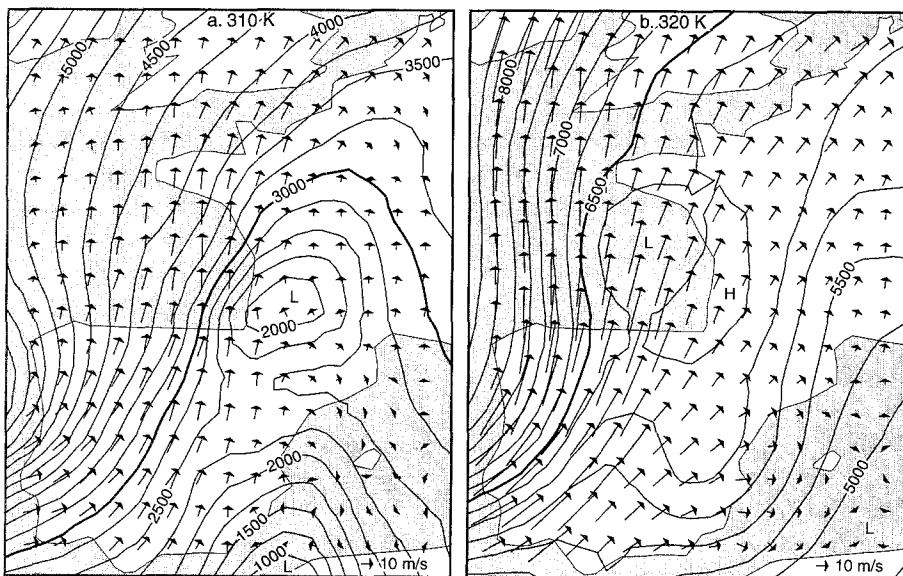


Fig. 14. Isopleths of the height of the 310 K isentropic surface (a) and the height of the 320 K isentropic surface (b), labeled in m, corresponding to August 8, 1992, 0600 UTC, derived from the ECMWF analysis on isobaric surfaces by linear interpolation. Also shown are wind vectors on the respective isentropic surfaces. The analysis has been smoothed using a nine-point filter

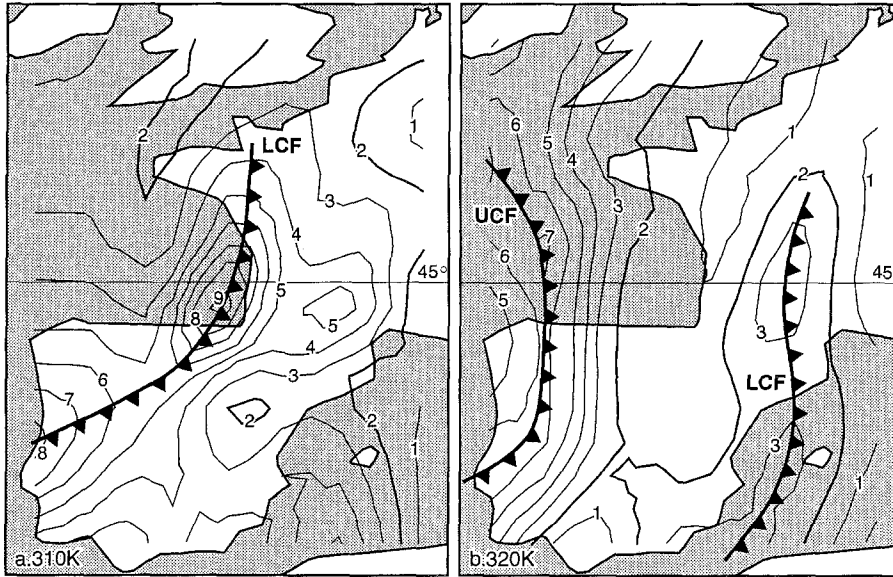


Fig. 15. Isopleths of the absolute value of the slope of the 310 K isentrope (a) and of the 320 K isentrope (b) (labeled in units of 10^{-3}), corresponding to August 8, 1992, 0600 UTC, derived from the ECMWF analysis. The analysis has been smoothed using a nine-point filter. The fronts LCF and UCF are explained in the text

in the satellite image in Fig. 2a. The front in the east on the 320 K surface is connected to the band of scattered clouds over eastern Iberia and southern France (see Fig. 2a–d). We will see in the next section that this front is in fact part of the LCF!

8. Relation Between Frontal Intensification and Destabilization

The rate of change of the intensity of a front oriented in the south-north (y) direction and moving with speed c in the x -direction is given by

$$\left[\frac{\partial I_{Fx}}{\partial t} \right]_{\text{rel}} = \frac{dI_{Fx}}{dt} - (u - c) \frac{\partial I_{Fx}}{\partial x} - w \frac{\partial I_{Fx}}{\partial z} \quad (2)$$

where the subscript “rel” indicates that the rate of change of I_{Fx} is evaluated in a reference frame moving in the x -direction with the same speed (c) of the front. We have assumed that

$$I_{Fy} = 0 \quad \text{and} \quad \frac{\partial I_{Fx}}{\partial y} = 0. \quad (3)$$

If we identify the actual position of the front with the location of the maximum in the absolute value of I_{Fx} , we may assert that

$$\frac{\partial I_{Fx}}{\partial x} = 0 \quad (4)$$

at the front, implying that the second term on the right hand side of (2) is equal to zero. The first term on the right hand side of (2) can be evaluated as follows (a derivation is given in appendix C):

$$\begin{aligned} \frac{dI_{Fx}}{dt} &= \frac{d}{dt} \left(\frac{-\partial\theta}{\partial x} \left[\frac{\partial\theta}{\partial z} \right]^{-1} \right) \\ &= -(I_{Fx})^2 \frac{\partial u}{\partial z} + I_{Fx} \frac{\partial w}{\partial z} - I_{Fx} \frac{\partial u}{\partial x} + \frac{\partial w}{\partial x}, \end{aligned} \quad (5)$$

provided

$$\frac{d\theta}{dt} = 0 \quad \text{and} \quad I_{Fy} = 0. \quad (6)$$

In Eqs. (2) and (5) we see that changes in the intensity of a front are induced by the following mechanisms:

- vertical shear of the horizontal component of the cross-frontal wind (first term on the r.h.s. of (5)), which tilts the isentropes to the vertical;
- divergence of the vertical wind or “stretching” (second term on the r.h.s. of (5)), which reduces the static stability;
- confluence of the cross-frontal wind (third term on the r.h.s. of (5)), which increases the horizontal potential temperature gradient;
- cross-frontal horizontal shear of the vertical wind (fourth term on the r.h.s. of (5)), which tilts the isentropes to the vertical;

- (e) vertical advection of frontal intensity (third term on the r.h.s. of (2)).
- (f) horizontal advection of frontal intensity (second term on the r.h.s. of (2), which, as mentioned earlier, vanishes at the front itself, but may be important in the vicinity of the front.

Only mechanism (d) is actually *frontogenetic*. The other mechanisms requires the existence of a front and, thus, can only induce changes in the intensity of an existing front. This is, incidentally, also termed frontogenesis or frontolysis by many authors (Miller, 1948; Pettersen, 1956; Holton, 1992).

Mechanisms (a) and (b), which induce a destabilization (of hydrostatic balance), are of interest for convection. They have no counterpart in the traditional approach to frontal intensification. This can be seen when we write down the equation for the rate of change of frontal intensity, defined by Miller (1948) as the rate of change of the horizontal gradient of θ following the motion. Restricting the analysis, again, to two dimensions (i.e. $\partial\theta/\partial y = 0$) and adiabatic conditions, we may write:

$$\frac{d}{dt} \left(\frac{\partial\theta}{\partial x} \right) = \frac{-\partial\theta}{\partial x} \frac{\partial u}{\partial x} - \frac{\partial\theta}{\partial z} \frac{\partial w}{\partial x}. \quad (7)$$

The first term on the right hand side of (7) is the counterpart of mechanism (c), while the second term is the counterpart of mechanism (d).

In the quasi-geostrophic approximation of frontal intensification, from which the x -component of the Q -vector is derived, only mechanism (c) is included (i.e. the third term on the right hand side of (5) and/or the first term on the right hand side of (7)), provided we again restrict the analysis to two dimensions.

Therefore, *the alternative definition (2) of frontogenesis contains the frontogenetic mechanisms found in the traditional approach*. Additional frontogenetic terms appear, however, related to the destabilization of the atmosphere, which make this new approach to frontogenesis very suitable for use in this study.

We will analyse the intensification of the front over the south of France, since here the squall line reaches its maximum intensity. We will choose the 45° N latitude circle, since the frontal system at this latitude is *approximately* oriented

in south-north direction (this approximation is better for the fronts on the 320 K surface (Fig. 15b) than for the front on the 310 K surface (Fig. 15a), it is sufficient to consider the slope of the isentropes with respect to x . If we *qualitatively* apply eqs (2) and (5) to the *cyclonic* vertical circulation within the Spanish plume as observed between 2° W and 5° E at 45° N in the cross-section depicted in Fig. 11a, we find that the “tilting mechanisms” (a) and (d) *intensify* the front *everywhere*, because $I_{Fx} < 0$, $\partial u/\partial z > 0$ and $\partial w/\partial x < 0$. Vertical stretching and horizontal convergence or confluence, i.e. mechanisms (b) and (c), induce frontal intensification near the earth’s surface on the cold (west) side of the circulation as well as aloft on the warm (east) side of the circulation because in these areas $\partial w/\partial z > 0$ and $\partial u/\partial x < 0$. These mechanisms will thus induce a *forward tilt of the front with height*.

The tendency towards a forward tilt with height of the front within the Spanish plume is confirmed by the ECMWF-analysis of the frontal intensity. Figure 16 shows a vertical/zonal cross section analysis of the frontal intensity, I_{Fx} for 45° N. In Fig. 16a, which corresponds to 0000 UTC the UCF and the LCF can clearly be distinguished. The forward tilt of the LCF at 45° N and 0600 UTC (see Fig. 16b) is particularly striking. If we compare figures 16a and 16b, we observe that the LCF not only intensifies, but also expands significantly in upward and eastward direction between 0000 UTC and 0600 UTC.

If we now apply Eqs. (2) and (5) to the *anticyclonic* vertical circulation within the region of cold air advection as observed at 45° N between 5° W and 2° W (see Fig. 10a and Fig. 11) we find that the “tilting mechanism” (d) will *weaken* the front *everywhere*, because $I_{Fx} < 0$ and $\partial w/\partial x > 0$. The effect of the other “tilting mechanism” (a) is less easily evaluated because the sign of the term $\partial u/\partial z$ is rather undefined. Mechanisms (b) and (c), will induce frontal intensification near the earth’s surface on the east side of the circulation as well as aloft on the west side of the circulation because in these areas $\partial w/\partial z > 0$ and $\partial u/\partial x < 0$. We may conclude that the front in the region of horizontal cold advection will tend to *weaken* and tilt backwards.

We now see, by comparing Fig. 15b and 16b, that the front on the 320 K surface over eastern

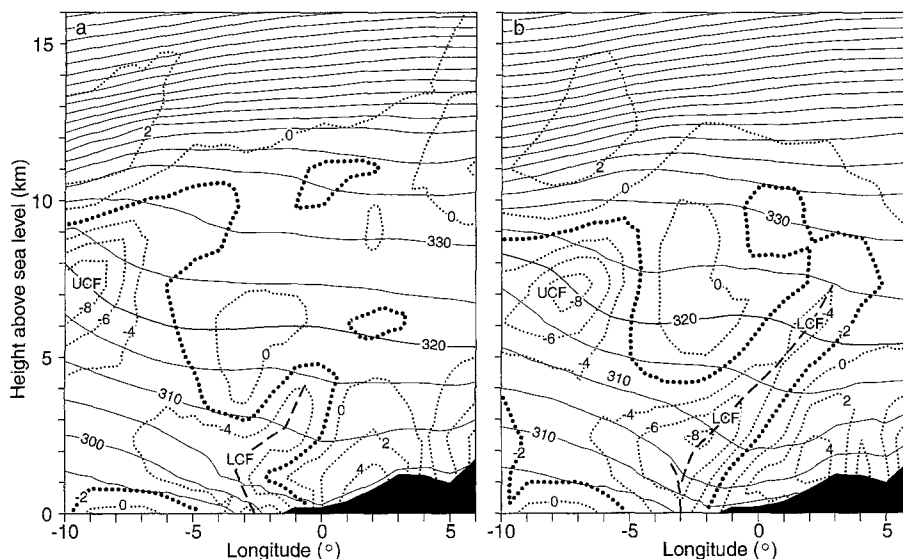


Fig. 16. Vertical cross section analysis of the slope of isentropes, $(\partial z/\partial x)_\theta$, along the 45° N latitude circle corresponding to August 8, 1992, 0000 UTC (a) and 0600 UTC (b), according to the ECMWF analysis. The orography of France, smoothed as in the ECMWF-model, is also shown. Isopleths of potential temperature are indicated by thin solid lines (labeled in K), and isopleths of $(\partial z/\partial x)_\theta$ are indicated by dotted lines, labeled in units of 10^{-3} . The dashed line indicates the axis of the lower cold front (LCF)

Iberia and southern France (see Fig. 15b) is in fact part of the LCF. The line of broken clouds observed in the satellite images in Fig. 2 in connection with this front probably consists of castellanus and floccus clouds (see Ludlam, 1980, plate 8.24). These type of clouds are frequently observed as a forerunner of a thunderstorm, and can thus be linked to the forward tilt and intensification of the LCF.

9. Distribution and Changes in Moist Static Stability

An important condition for the occurrence of deep convection is potential static instability ($\partial\theta_e/\partial z < 0$) up to great heights. The cross-frontal vertical circulation in the region of warm advection (the Spanish plume) can create this condition. This is illustrated in Fig. 17, which shows an analysis of the equivalent potential temperature in a vertical/zonal cross section at 42° N (over northern Iberia), at 00 UTC and at 12 UTC. According to Fig. 3, the explosive convective development occurred first at this latitude at and or shortly after 1200 UTC, at

3° W. The LCF is recognized in Fig. 17, which should be compared with Fig. 11a, by the crowding of the approximately vertically oriented isopleths of θ_e . The leading edge of this front at the earth's surface coincides approximately with the 325 K isopleth. To the east (over eastern Iberia) the stratification is potentially unstable up to a height of at least 8 km, while to the west, within the cooler air behind the front only the lowest 3 km are potentially unstable. The convergence/confluence line, so clearly recognizable at the earth's surface (see Fig. 5), apparently extends up to a height of approximately 2–3 km above sea level. It is located within the potentially warm air, although, between 000 UTC and 1200 UTC the cold front at the earth's surface appears to take over the convergence/confluence line. Above this height, up to a height of about 7500 m, we can observe, if we compare Fig. 17a and 17b, a decrease of θ_e between 0000 and 1200 UTC. This appears to be caused by the enhanced westerly component of the wind, associated with the eastern (cyclonic) branch of the cross-frontal circulation, which advects air with low θ_e from the west.

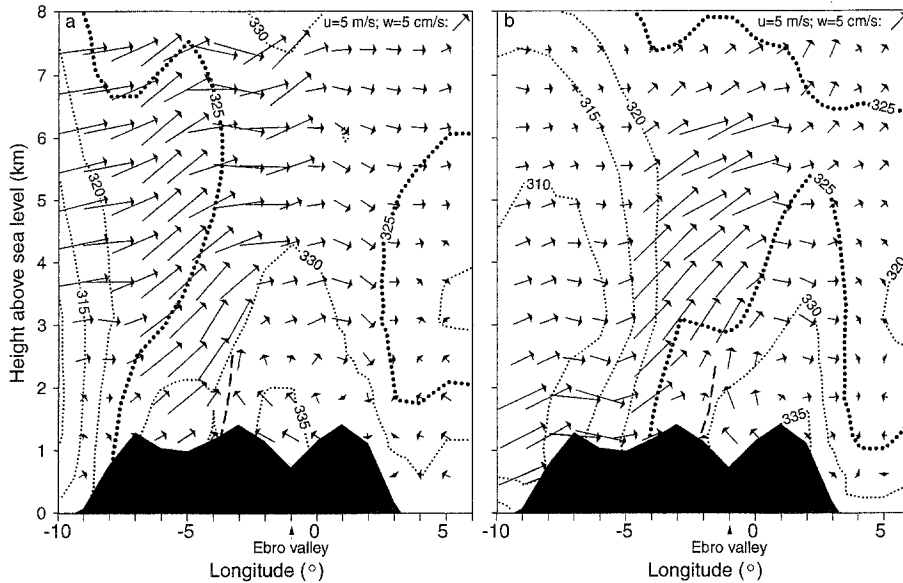


Fig. 17. Vertical cross section analysis of the equivalent potential temperature (dotted lines, labeled in K) and the component of the wind vector in the plane of the cross section along the 42° N latitude circle corresponding to August 8, 1992, 0600 UTC, according to the ECMWF analysis. The orography of Iberia at this latitude, smoothed as in the ECMWF-model, is also shown. The dashed line indicates the position of the convergence/confluence line (see also Fig. 5)

10. Conclusion

The thundery low in western Europe is a product of an adjustment process in the lower troposphere of the jet-front system as it approaches the hot continent from the cool Atlantic Ocean. In advance of the cold front very warm air is advected from the south (the so-called Spanish Plume). The sharp horizontal gradient in temperature advection induces frontal intensification. Readjustment to thermal wind balance is accompanied by a cross-frontal circulation with upward motion at the leading edge of the front. This is a decisive factor in triggering the squall line. Others, such as Means (1952) and Browning and Pardoe (1973), have also found that bands of vigorous convection at a surface cold front are frequently associated with a low level jet consisting of a tongue of anomalously warm air.

The events leading up to the formation of the prefrontal squall line within the thundery low are interpreted using the slope of isentropes as indicator of frontal intensity. An equation is derived for the rate of change in time of frontal intensity, which predicts a forward tilt of the cold front with increasing height due to the “frontogenetic” effect of the cross-frontal circulation in the area of warm air advection. Associated with this, the atmosphere at mid-tropospheric levels is destabilized. This interpretation is supported by

the ECMWF-analyses of the case of August 8, 1992.

Acknowledgements

I would like to thank Seijo Kruizinga (KNMI, De Bilt) for helping me obtain the data for this study and three reviewers of the earlier version of this article for helpful comments.

Appendix A: Analysis Scheme for Surface Observations

The analysis of the sea level pressure (see Fig. 4) has been performed by computer using “optimum” linear interpolation to a grid of 36 (x) by 41 (y) points stretching from 11° W to 10° E and from 37° N to 55° N. Therefore, the grid distance is 0.45° in the meridional (y) direction and 0.6° in the zonal (x) direction. A grid point value of the pressure is obtained by piecewise linear interpolation using the values measured at three points in the neighbourhood (Pedder, 1981). For each gridpoint the nearest nine stations, giving “reasonable” measurements, are found. All possible permutations of three stations are formed from the nine stations. This yields 84 overlapping station-triangles. If a triangle contains an angle smaller than 25° it is discarded, yielding $N \leq 84$ station triangles and N corresponding values of the pressure at the gridpoint. From this set of N values a histogram is constructed. The range of data is divided into class intervals or “bins” of 1 hPa, and the number of values falling into each bin is counted. One “optimal” value is selected from the bin containing the maximum number of values. The value is optimal in the sense that it is calculated from measurements made at three stations lying at the

minimum mean distance from the gridpoint. The resulting analysis is smoothed four times in a row with a 9 gridpoint smoother (see Haltiner and Martin, 1980, p. 397).

Appendix B: Moisture Flux Convergence at the Earth's Surface

The conservation equation for water vapour is,

$$\frac{\partial \rho q}{\partial t} = - \left(\frac{\partial \rho u q}{\partial x} + \frac{\partial \rho v q}{\partial y} \right) - \frac{\partial \rho w q}{\partial z} + \text{sources.}$$

Here q is the specific humidity. The local change in specific humidity with respect to time is thus determined by the horizontal moisture flux divergence (the first term between brackets on the r.h.s.), the vertical moisture flux divergence (the second term on the r.h.s.) and by external sources of water vapour. The latter term 'sources' on the right hand side stands for local sources of water vapour, such as evaporation from the earth's surface, evaporation of precipitation and condensation of water vapour. The horizontal moisture flux divergence can be analysed from the surface data. This is done by interpolating the measured values of $\rho u q$ and $\rho v q$ to a grid using the scheme described in the appendix A. This scheme yields the gradients of $\rho u q$ and $\rho v q$ (and thus also the horizontal moisture flux divergence) at the gridpoints directly from the measurements. The analysis shown in Fig. 6 is smoothed four times in a row with a 9 gridpoint smoother (see Haltiner and Martin, 1980).

Appendix C: Derivation of Frontogenesis Equation (5)

Let us define the slope of an isopleth of a variable S by

$$I_{Fx} \equiv \left(\frac{\partial z}{\partial x} \right)_s = - \frac{\partial S}{\partial x} \left[\frac{\partial S}{\partial z} \right]^{-1}.$$

The material change of this slope is given by

$$\frac{d}{dt} I_{Fx} = \frac{\partial S}{\partial x} \left(\frac{\partial S}{\partial z} \right)^{-2} \frac{d}{dt} \left(\frac{\partial S}{\partial z} \right) - \left(\frac{\partial S}{\partial z} \right)^{-1} \frac{d}{dt} \left(\frac{\partial S}{\partial x} \right).$$

If $\frac{dS}{dt} = 0$ then

$$\begin{aligned} \frac{d}{dt} I_{Fx} = & - \frac{\partial S}{\partial x} \left(\frac{\partial S}{\partial z} \right)^{-2} \left(\frac{\partial S}{\partial x} \frac{\partial u}{\partial z} + \frac{\partial S}{\partial y} \frac{\partial v}{\partial z} + \frac{\partial S}{\partial z} \frac{\partial w}{\partial z} \right) \\ & + \left(\frac{\partial S}{\partial z} \right)^{-1} \left(\frac{\partial S}{\partial x} \frac{\partial u}{\partial x} + \frac{\partial S}{\partial y} \frac{\partial v}{\partial x} + \frac{\partial S}{\partial z} \frac{\partial w}{\partial x} \right). \end{aligned}$$

or

$$\begin{aligned} \frac{d}{dt} I_{Fx} = & I_{Fx} \left(-I_{Fx} \frac{\partial u}{\partial z} - I_{Fy} \frac{\partial v}{\partial z} + \frac{\partial w}{\partial z} \right) \\ & + \left(-I_{Fy} \frac{\partial u}{\partial x} - I_{Fy} \frac{\partial v}{\partial x} + \frac{\partial w}{\partial x} \right), \end{aligned}$$

where

$$I_{Fy} \equiv \left(\frac{\partial z}{\partial y} \right)_s = - \frac{\partial S}{\partial y} \left[\frac{\partial S}{\partial z} \right]^{-1}.$$

If $I_{Fy} = 0$ then

$$\frac{d}{dt} I_{Fx} = - (I_{Fx})^2 \frac{\partial u}{\partial z} + I_{Fx} \frac{\partial w}{\partial z} - I_{Fx} \frac{\partial u}{\partial x} + \frac{\partial w}{\partial x},$$

which corresponds to Eq. 5 in section 8, with $S \equiv \theta$.

References

- Alberoni, P. P., Nanni, S., Crespi, M., Monai, M., 1996: The supercell thunderstorms on 8 June 1990: mesoscale and radar observations. *Meteorol. Atmos. Phys.*, **58**, 123–138.
- Browning, K. A., Pardoe, G. W., 1973: Structure of low-level jetstreams ahead of mid-latitude cold fronts. *Quart. J. Roy. Meteor. Soc.*, **99**, 619–638.
- Browning, K. A., Roberts, N. M., 1994: Use of satellite imagery to diagnose events leading to frontal thunderstorms: part 1 of a case study. *Met. Apps.*, **1**, 303–310.
- Browning, K. A., Hill, F. F., 1984: Structure and evolution of a mesoscale convective system near the British Isles. *Quart. J. Roy. Meteor. Soc.*, **110**, 897–913.
- Carlson, T. N., Ludlam, F. H., 1968: Conditions for the occurrence of severe local storms. *Tellus*, **20**, 203–226.
- Collier, C. G., Lilley, R. B. E., 1994: Forecasting thunderstorm initiation in northwest Europe using thermodynamic indices, satellite and radar data. *Met. Apps.*, **1**, 75–84.
- Delden, A. van, 1992: The dynamics of meso-scale atmospheric circulations. *Physics Reports*, **211**, 251–376.
- Delden, A. van, 1994: Jetstreak- and trough-dynamics and meso-scale flow features during the development of "thunderly lows" in Western Europe. In: *The Life Cycles of Extratropical Cyclones*, vol. 2. Proceedings of an International Symposium, Bergen Norway. pp. 346–352.
- Galvin, J. F. P., Bennett, P. H., Couchman, P. B., 1995: Two thunderstorms in summer 1994 at Birmingham. *Weather*, **50**, 239–250.
- Haltiner, G. J., Williams, R. T., 1980: *Numerical Prediction and Dynamic Meteorology*, 2nd edn. New York: John Wiley, 477 pp.
- Haase-Straub, S. P., Hagen, M., Hauf, T., Heimann, D., Peristeri, M., Smith, R. K., 1997: The squall line of 21 July 1992 in Southern Germany: an observational study. *Beitr. Phys. Atmos.*, **70**, 147–165.
- Heimann, D., Kurz, M., 1985: The Munich hailstorm of July 12, 1984: Discussion of the synoptic situation. *Beitr. Phys. Atmos.*, **58**, 528–544.
- Höller, H., 1994: Mesoscale Organization and Haifall characteristics of deep convection in southern Germany. *Beitr. Phys. Atmos.*, **67**, 219–234.
- Höller, H., Reinhardt, M. E., 1986: The Munich hailstorm of July 12, 1984 – Convective development and preliminary hailstone analysis. *Beitr. Phys. Atmos.*, **59**, 1–12.
- Holton, J. R., 1992: *An Introduction to Dynamic Meteorology*, 3rd edn. San Diego: Academic Press, 510 pp.
- Joe, P., Crozier, C., Donaldson, N., Etkin, D., Clodman, S., Abraham, J., Siok, S., Biron, H-P., Leduc, M., Chadwick, P., Knott, S., Archibald, J., Vickers, G., Blackwell, S., Drouillard, R., Whitman, A., Brooks, H., Kouwen, N., Verret, R., Fournier, G., KochuBajda, B., 1995: Recent progress in operational forecasting of severe summer weather. *Atmosphere-Ocean*, **33**, 249–302.

- Kurz, M., 1993: Severe thunderstorms over western Germany – a case-study of the weather situation on 20 August 1992. *Meteor. Magazine*, **122**, 177–188.
- Ludlam, F. H., 1980: *Clouds and Storms*. University Park: Pennsylvania University Press, 405 pp.
- Means, L. L., 1952: On thunderstorm forecasting in central U. S. *Mon. Wea. Rev.*, **80**, 165–189.
- McCallum, E., Waters, A. J., 1993: Severe thunderstorms over south-east England 20/21 July 1992: satellite and radar perspective of a mesoscale convective system. *Weather*, **48**, 198.
- Miller, J. E., 1948: On the concept of frontogenesis. *J. Meteor.*, **5**, 196–171.
- Morris, R. M., 1986: The Spanish plume- testing the forecaster's nerve. *Meteor. Magazine*, **115**, 349–357.
- Pedder, M. A., 1981: Practical analysis of dynamical and kinematic structure: principles, practice and errors. In: Atkinson, B. W., (ed.) *Dynamical Meteorology: An Introductory Selection*. London: Methuen & Co., pp. 55–68.
- Petterssen, S., 1940: *Weather Analysis and Forecasting*, 1st edn. New York: MacGraw-Hill, 503 pp.
- Petterssen, S., 1956: *Weather Analysis and Forecasting*, 2nd edn. New York: MacGraw-Hill.
- Prenosil, T., Thiel, D., Kraus, H., 1995: Frontogenesis and cross frontal circulation in a strong summertime cold front. *Meteorol. Atmos. Phys.*, **56**, 181–196.
- Ramis, C., Llasat, M. C., Genovés, A., Jansá, A., 1994: The October-1987 floods in Catalonia: synoptic and mesoscale mechanisms. *Met. Apps.*, **1**, 337–350.
- Schiesser, H. H., Houze Jr., R. A., Huntrieser, H., 1995: The mesoscale structure of severe precipitation systems in Switzerland. *Mon. Wea. Rev.*, **123**, 2070–2097.
- Schmid, W., Schiesser, H.-H., Bauer-Messmer, B., 1997: Supercell storms in Switzerland: case studies and implications for nowcasting severe winds with Doppler radar. *Meteorol. Appl.*, **4**, 49–67.
- Sénési, S., Bougeault, P., Chéze, J.-L., Consentino, P., Thepenier, R.-M., 1996: The Vaison-La-Romaine flash flood: mesoscale analysis and predictability issues. *Wea. Forecasting*, **11**, 417–442.
- Young, M. V., 1995: Severe thunderstorms over south-east England on 24 June 1994. *Weather*, **50**, 250–256.

Author's address: Aarnout van Delden, Institute of Marine and Atmospheric Research Utrecht, University of Utrecht, Princetonplein 5, NL – 3584 CC Utrecht, The Netherlands.